JOURNAL OF SPACECRAFT AND ROCKETS
Vol. 29, No. 4, July-August 1992

Impulse Response of Space Reflectors with Localized Modes

Phillip J. Cornwell* and Oddvar O. Bendiksen†
Princeton University, Princeton, New Jersey 08544

The forced response in a generic class of disordered large space reflectors that have both localized and extended modes is presented. Localization is characterized by the amplitude of a global mode becoming confined to a local region of the structure. This investigation examines the disturbance propagation associated with the impulsive loading of one substructure, as would be the case with a rock (or micrometeor) hitting a rib or a single actuator acting on a rib. For the 18-rib reflector studied, if the first mode group (which is primarily first bending) is not localized, then the disturbance was found to propagate throughout both the perfect and imperfect structures with very little difference between the two cases. When the first mode group is localized, a spatial decay of the vibration amplitude along the structure was observed wtih the energy being confined near the source of excitation.

Nomenclature

A = cross-sectional area of axial member
EI = rib flexural rigidity
F_0 = magnitude of impulsive load
$[K]$ = global stiffness matrix
k_{ij}^a = effective stiffness of axial member
ℓ = total length of rib
ℓ_a = length of axial member
$[M]$ = global mass matrix
m = rib mass per unit length
N = total number of ribs
N_a = number of axial members between ribs
n = circumferential wave number
p = number of degrees of freedom per substructure
Q_i = generalized force
q_i = generalized coordinate
$\bar{q}_i$ = amplitude of q_i
r = imperfection strength
T = total kinetic energy
T_0 = cable pretension
t = time
U = total potential energy
V_{ij} = potential energy due to the jth axial member between rib i and $i+1$
$v(x, t)$ = displacement of in-plane motion
$w(x, t)$ = displacement of out-of-plane motion
$\bar{x}$ = x/ℓ
α_i, β_i = constants in assumed mode shapes
$\Delta\lambda$ = normalized eigenvalue band
θ = half-angle between ribs
λ = eigenvalue, $(\omega/\omega_0)^2$
τ = nondimensional time, $t\omega_0$
$\phi_n(x)$ = mode shape function
$[\Psi]$ = matrix of eigenvectors
ψ_n = eigenvector
ω = natural frequency
ω_0 = reference frequency, $\sqrt{EI/m\ell^4}$
$\bar{\omega}$ = nondimensional frequency, ω/ω_0

Presented as Paper 89-1180 at the 30th Structures, Structural Dynamics and Materials Conference, Mobile, AL, April 3-5, 1989. Received March 2, 1990; revision received Jan. 14, 1991; accepted for publication Jan. 29, 1991.

*Graduate Student, Department of Mechanical and Aerospace Engineering; currently Assistant Professor, Mechanical Engineering Department, Rose-Hulman Institute of Technology, Terre Haute, Indiana 47803. Member AIAA.

†Assistant Professor, Department of Mechanical and Aerospace Engineering; currently Associate Professor, Mechanical, Aerospace, and Nuclear Engineering Department, University of California, Los Angeles, Los Angeles, California 90024. Member AIAA.

Introduction

THANKS to the continuing improvement in computers, structural dynamics problems that used to be intractable are now being solved numerically on a routine basis. Numerical methods of analysis have allowed mathematical models based on the most simplified assumptions to be replaced with models with more realistic assumptions. Nonlinear effects and extremely complex geometries can now be modeled. Curiously absent from the process of making many models more realistic have been variations within a structure due to factors such as manufacturing or assembly errors. The implicit rationale for this omission is that the effect will be small; that is, qualitatively the results should be the same. Another reason for neglecting structural imperfections in structures with cyclic symmetry or some form of periodicity is the tremendous computational advantage. Very efficient analytical techniques have been developed that take full advantage of periodicity and reduce significantly the number of computations required.[1-3] Recently, however, some periodic structures that are characterized by a number of weakly coupled substructures have been shown to be quite sensitive to structural imperfections,[2,4,9] and natural modes that were originally extended throughout the structure become localized to a small region of the structure.

Large flexible space structures, such as large space reflectors, which are characterized by high modal densities, have been found to be susceptible to mode localization.[8] Because such structures often have extremely stringent pointing and shape requirements, some method of actively controlling the

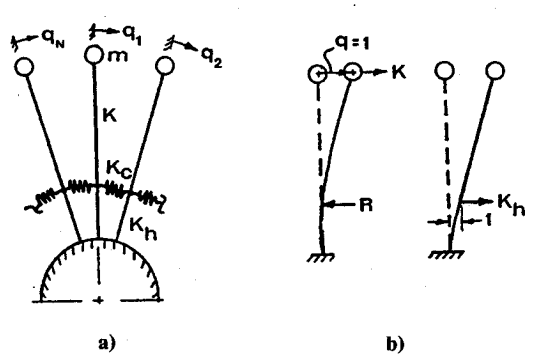

Fig. 1 a) Simple model of a structure with cyclic symmetry, and b) substructure (beam) stiffness coefficients.

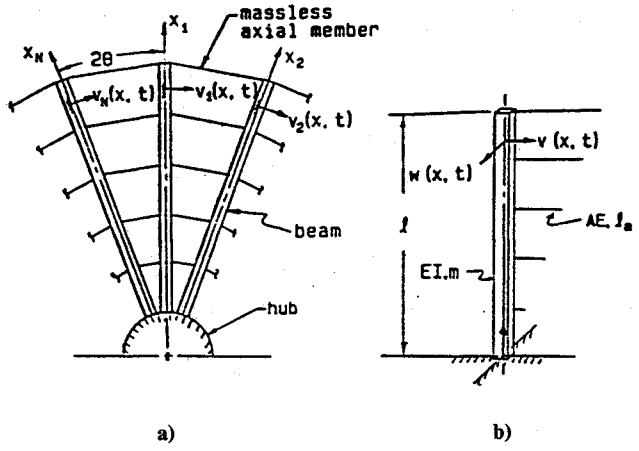

Fig. 2 a) Structural model for a radial rib reflector/antenna, and b) typical substructure consisting of rib beam and sectional wires (axial members).

structure becomes necessary. If the control system designs are based on the extended modes of the perfect structure, serious problems could result concerning robustness and stability if the true structure has localized modes. It has also been proposed that mode localization may have some beneficial consequences as a means of passive control of vibration propagation. These questions can only be resolved by examining the forced response problem of a realistic engineering structure.

The forced vibration problem has been examined in structures with single-degree-of-freedom (SDOF) substructures.[4,10,11] Localization in SDOF systems has been found to manifest itself by a spatial decay of the vibrational amplitude along the structure with the energy being confined near the source of the excitation. Hodges and Woodhouse have presented an analysis of this phenomenon for a simple infinite one-dimensional structure.[12] Pierre and Cha have also illustrated this phenomenon by applying a single harmonic excitation at one of a chain of coupled oscillators.[9] For the perfect structure, the excitation is found to propagate throughout the structure, provided the excitation lies within the passband of the structure.

This paper is an extension of the investigation initiated in Ref. 8, where the confinement of traveling waves was demonstrated using the SDOF per substructure model of a cyclic structure shown in Fig. 1. The structure was shown to have strongly localized modes. In Ref. 8, the wave confinement by structural irregularities was studied by solving the initial value problem associated with applying the initial conditions corresponding to a right-running wave. The conclusion was that for finite engineering structures that have strongly localized modes, the wave confinement phenomenon does indeed appear to exist.

The objective of the present paper is to extend the study of Ref. 8 to multi-degree-of-freedom (MDOF) substructures where instead of solving the initial value problem, the impulse response problem is examined. Impulsive loading is applied to one substructure as would be the case with a rock (or micrometeor) hitting a rib or a single actuator acting on the rib. To our knowledge, this represents the first time that the impulse response problem has been examined for a realistic engineering structure that has both extended and localized modes.

Structural Models

For the class of axially symmetric structures considered in this study, Figs. 2, the basic substructure consists of one of the N radial beams (ribs) with the associated wire mesh, Fig. 2b. The structural model used for most of the analysis is a Rayleigh-Ritz model based on the first five cantilever beam bending modes for each radial rib. The wire mesh or web membrane between the ribs is modeled as a number of massless axial members (springs) attached at specific points, as illustrated in Figs. 2. For the impulsive loading of a single rib, the hub of the reflector is considered to be fixed. The response problem is solved using modal analysis.

The cross section of the ribs is assumed to be symmetric, and the reflector is considered to be flat so that the in-plane and out-of-plane motions decouple for small amplitude vibration. The vibration displacement of the beam in the plane of the reflector is denoted by $v_i(x,y)$ (Fig. 2b).

For the Rayleigh-Ritz model, the in-plane displacement of a rib can be written as

$$v_i(x,t) = \sum_{n=1}^{5} q_n(t)\phi_n(x) = \{q\}_i^T\{\phi\} \tag{1}$$

The mode shapes used in the study are given by

$$\phi_n = \cosh \beta_n\bar{x} - \cos \beta_n\bar{x} - \alpha_n(\sinh \beta_n\bar{x} - \sin \beta_n\bar{x}) \tag{2}$$

where

$$\begin{aligned} \beta_1 &= 1.875104, & \alpha_1 &= 0.7340955 \\ \beta_2 &= 4.694091, & \alpha_2 &= 1.018466 \\ \beta_3 &= 7.854757, & \alpha_3 &= 0.9992245 \\ \beta_4 &= 10.99554, & \alpha_4 &= 1.000034 \\ \beta_5 &= 14.13717, & \alpha_5 &= 0.9999986 \end{aligned} \tag{3}$$

The total kinetic energy is

$$T = \sum_{i=1}^{N} T_i = \sum_{i=1}^{N} \frac{1}{2}\{\dot{q}\}_i^T[M]_i\{\dot{q}\}_i \tag{4}$$

where

$$[M]_i = \int_0^{\ell} m_i\{\phi\}\{\phi\}^T\,dx \tag{5}$$

The total potential energy can be written as a sum of the strain energy due to bending of the beams and the strain energy in the axial members between the beams:

$$U = \sum_{i=1}^{N} \frac{1}{2}\{q\}_i^T[K]_i\{q\}_i + \sum_{i=1}^{N}\sum_{j=1}^{N_a} V_{ij} \tag{6}$$

where

$$[K]_i = \int_0^{\ell} EI_i\{\phi''\}\{\phi''\}^T\,dx \tag{7}$$

and V_{ij} is the energy associated with the jth axial member between ribs i and $i+1$. If the axial members have a force-dis-

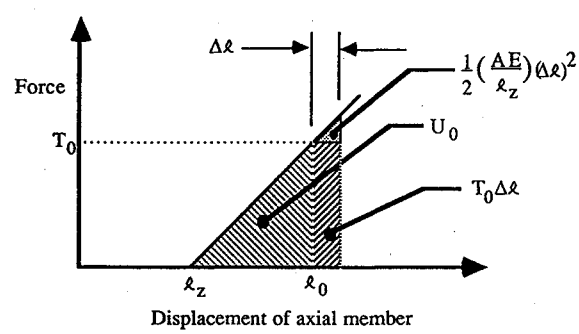

Fig. 3 Force-displacement relationship for the connecting axial members; the axial members are assumed to be cables with an unstretched length of ℓ_z.

placement relationship as shown in Fig. 3, then the potential energy associated with the pretensioned axial member is

$$V_{ij} = \frac{1}{2}\left(\frac{AE}{\ell_z}\right)_{ij}(\Delta\ell_{ij}) + T_0(\Delta\ell_{ij}) + U_0 \tag{8}$$

where $(AE/\ell_z)_{ij}$ is the slope in Fig. 3 and T_0 is the pretension and is equal to

$$T_0 = (\ell_0 - \ell_z)\left(\frac{AE}{\ell_z}\right)_{ij} \tag{9}$$

where ℓ_z is the unstrained length of the cable and ℓ_0 is determined by the final geometry. For a flat antenna, the change in length of the axial member $\Delta\ell_{ij}$ is found to be

$$\Delta\ell_{ij} = [v_{i+1}(h_j,t) - v_i(h_j,t)]\cos\theta - \frac{1}{2\ell_{a_j}}[v_{i+1}(h_j,t) - v_i(h_j,t)]^2 \sin^2\theta \tag{10}$$

where $\ell_{a_j} = 2h_j \sin\theta$. Substituting Eq. (10) into Eq. (8) and keeping only the quadratic terms (which result in linear terms after applying Lagrange's equations), Eq. (8) reduces to

$$V_{ij} = \frac{1}{2}\left[\left(\frac{AE}{\ell_z}\right)_{ij}\cos^2\theta - \left(\frac{T_0}{\ell_a}\right)_{ij}\sin^2\theta\right][v_{i+1}(h_j,t) - v_i(h_j,t)]^2 \tag{11}$$

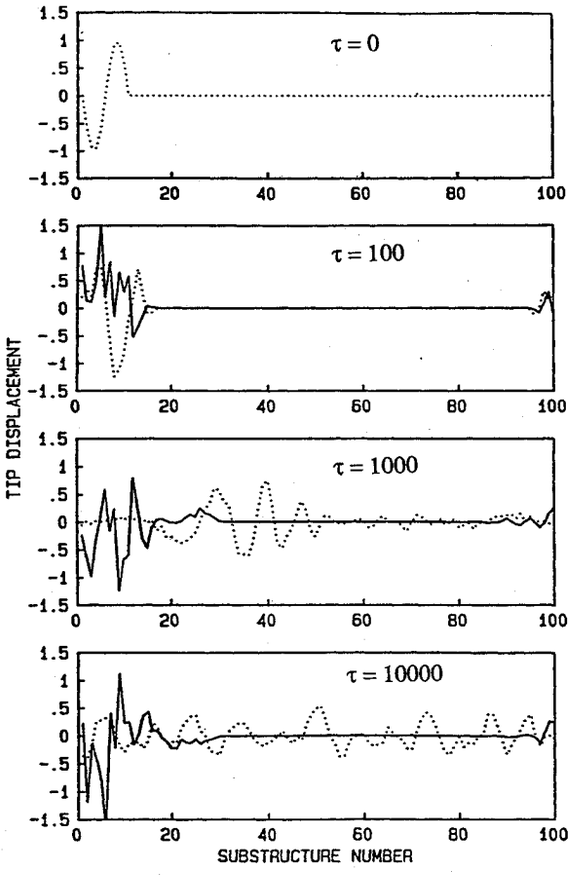

Fig. 4 Confinement of vibration by structural irregularities. Original local wave packet traveling right eventually becomes distributed over the entire structure if the structure is perfectly periodic (dotted line). When the structure is imperfect (solid line = ± 2.5% imperfections in k), a large region exists where the substructure amplitudes remain negligible, indicating that the original wave packet is trapped.

Table 1 Natural frequencies (Hz) of the first rib in-plane bending mode of the 15m (18-rib) reflector vs circumferential wave number n

n	El-Raheb and Wagner[14]	Present model	Difference, %
0	3.7590	3.7590	0
1	3.7813	3.7808	0.013
2	3.8440	3.8428	0.031
3	3.9367	3.9355	0.030
4	4.0465	4.0461	0.010
5	4.1594	4.1601	− 0.016

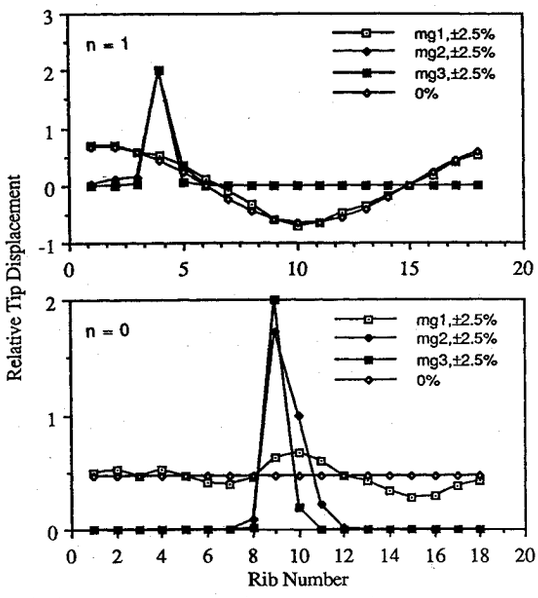

Fig. 5 Mode shapes of the $n = 0$ and 1 modes of the first mode group. Note the severe localization of the second and third mode groups; $N = 18$, $k_a = 0.298\ EI/\ell^3$.

$$= \tfrac{1}{2}k_{ij}^a[v_{i+1}(h_j,t) - v_i(h_j,t)]^2 \tag{12}$$

$$= \tfrac{1}{2}k_{ij}^a(\{q\}_i^T\{\phi\}|_{h_j} - \{q\}_{i+1}^T\{\phi\}|_{h_j})^2 \tag{13}$$

where

$$k_{ij}^a = \left[\left(\frac{AE}{\ell_z}\right)_{ij}\cos^2\theta - \left(\frac{T_0}{\ell_a}\right)_{ij}\sin^2\theta\right] \tag{14}$$

is the effective stiffness of the jth spring between beams i and $i+1$. In Ref. 8, it was shown that using multiple connecting wires does not change the shape of the natural modes significantly, provided the effective coupling remains the same. Therefore, only a single axial member will be used to model the wire mesh in this study. Previous studies[4,12] have shown that the variation in the coupling k_{ij}^a has a very small effect on the dynamics in comparison to variations in the flexural rigidity EI and will therefore be considered a constant, $k_{ij}^a = k^a =$ const. A random variation is introduced into the flexural rigidity such that

$$EI_i = EI_0(1 + P_i) \tag{15}$$

where P_i is a random variable having a uniform distribution between r and $-r$ where r is defined to be the imperfection strength. The equations of motion can be obtained by substituting Eqs. (4-14) into Lagrange's equations, resulting in a system of $5N \times 5N$ equations

$$[M]\{\ddot{q}\} + [K]\{q\} = \{Q\} \tag{16}$$

when we assume zero initial conditions and use the nondimensional time $\tau = \omega_0 t$, where $\bar{\omega}$ is the nondimensional frequency defined earlier. Once $\{\eta\}$ is calculated, the entire displacement field can be calculated using Eqs. (20) and (1).

The procedure for deriving the equations of motion is identical to the formulation used for the in-plane motion, except that the effective spring stiffness given by Eq. (14) will be different. Considering only the out-of-plane motion, the potential energy of the axial members can be written as

$$V_{ij} = \frac{1}{2}\left(\frac{T_0}{\ell_a}\right)_{ij} [w_{i+1}(h_j,t) - w_i(h_j,t)]^2 \tag{31}$$

so the effective spring stiffness is

$$k_{ij}^a = \left(\frac{T_0}{\ell_a}\right)_{ij} \tag{32}$$

Numerical Results and Discussion

In Ref. 8, the basic characteristics of wave confinement were illustrated using the simple model shown in Fig. 1 that has SDOF substructures and $N = 100$. The structural coupling between the structures was modeled by spring K_c, and hub springs K_h were introduced to extend the structural coupling beyond next neighbors. A sinusoidal wave was started over 10 of the substructures at $t = 0$, with initial conditions corresponding to a right-running wave. When random imperfections of $\pm 2.5\%$ were introduced in the substructure stiffness,

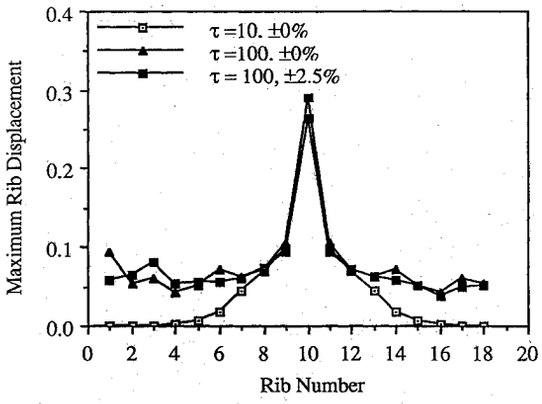

Fig. 9 Same as Fig. 8 except the maximum tip displacements are shown, illustrating that all the ribs are excited by $\tau = 100$ in both the perfect and imperfect structures.

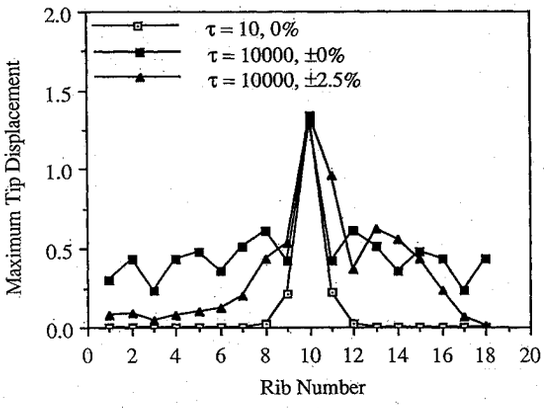

Fig. 10 Illustration of the effect that the location of the connecting member has on the disturbance propagation. The axial members are located between the midpoints of the ribs, and an impulsive load is applied to the midpoint of the 10th rib. Note that the displacements of the ribs furthest from the source of excitation remain small, although they are excited a small amount.

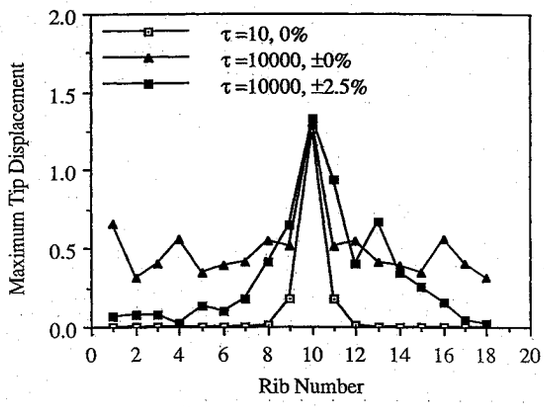

Fig. 11 Impulsive loading of the 10th rib with $k_a = 0.03EI/\ell^3$ and the axial member located at the tip of the ribs. Note that the excitation does not propagate throughout the structure when imperfections are introduced and is confined near the source of excitation.

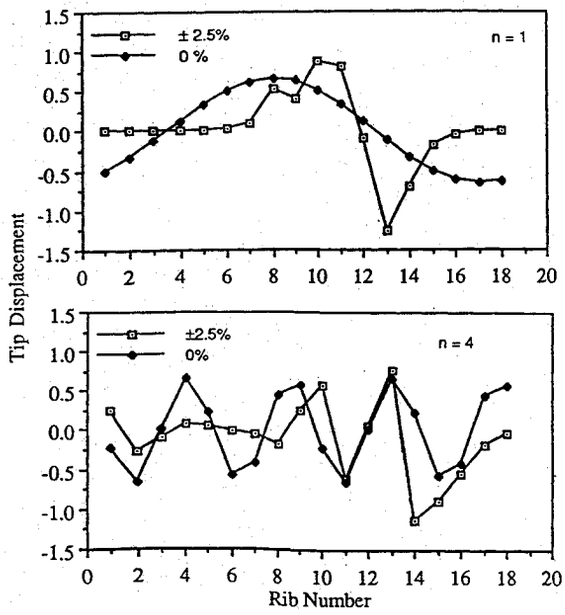

Fig. 12 The $n = 0$ and 4 modes for the same structure as shown in Fig. 11. Note that the modes of the first mode group are not localized on a single rib so one would not necessarily expect the energy to become confined to a local region as was the case shown in Fig. 11.

k, the vibrating behavior of the structure was found to change dramatically as shown in Fig. 4. For the perfect structure, the original "wave packet" eventually spreads throughout the structure, whereas for the structure with random imperfections, the vibrational energy remains confined to a well-defined local region of the structure. This confinement phenomenon was also observed when only one substructure was set in motion (plucked).

Illustrative results for impulsive loading in the plane of the reflector for an 18-rib structure are shown in Figs. 5-10 using the Rayleigh-Ritz formulation. Unless otherwise noted, the imperfect structure refers to a $\pm 2.5\%$ random variation in the flexural rigidity. The stiffness of the wire mesh was selected such that the frequency vs circumferential wave number n of the first in-plane bending mode matched the corresponding mode in Ref. 13. This resulted in an effective stiffness of $k^a = 0.298\ EI/\ell^3$. A comparison of the frequency matching is shown in Table 1. Clearly, the basic frequency vs circumferential wave number is captured very well. The in-plane results are presented initially because only the low-frequency in-plane modes are reported in Ref. 13. The natural frequencies were found to be clustered in mode groups. In the first mode group, the ribs are primarily in first bending. Similarly, the ribs in the

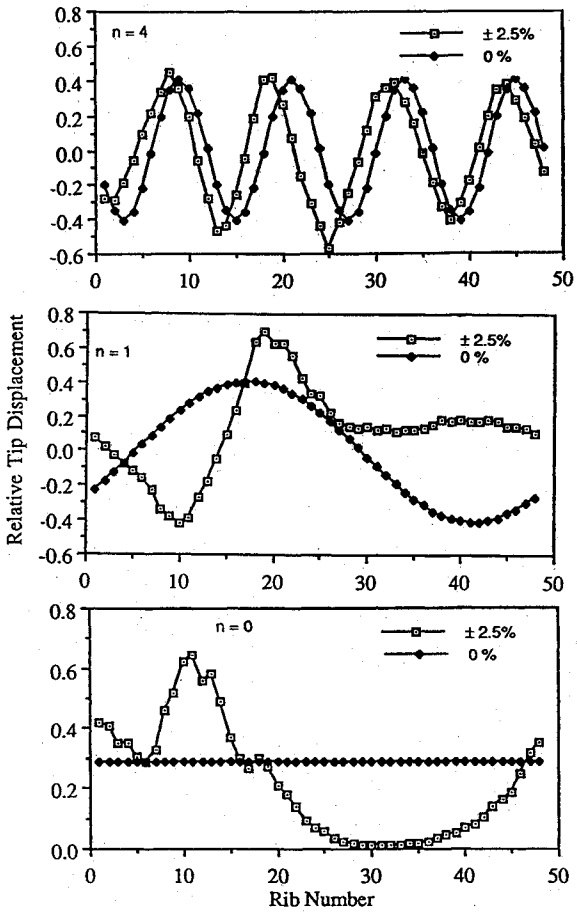

Fig. 13 Mode shapes for the $n = 0$, 1, and 4 modes of a 48-rib reflector, $k_a = 0.298\ EI/\ell^3$. Note that the $n = 0$ and 1 modes have suffered severe distortion in contrast to the $n = 4$ mode, which is just slightly perturbed.

second and third mode group are primarily in second and third bending, respectively. For an imperfection strength of ±2.5%, it was shown in Ref. 8 that the first mode group did not localize but the second and third mode groups did, with the localization becoming progressively more severe with increasing mode number. The $n = 0$ and 1 modes for the first three mode groups are shown in Fig. 5. Note the severe localization of the mode for the second and third mode groups. In Fig. 6 an impulsive load was applied to the tip of the 10th rib, and the coupling between ribs is provided by a single axial member between the tips of the ribs. The ribs are plotted as a linear chain in Fig. 6 merely for convenience in presenting the results. The displacement of the ribs is also exaggerated for clarity. Recall that the ribs at the right and left ends of the graph are connected to each other. The nondimensional time τ is obtained by multiplying the time by $\sqrt{EI/m\ell^4}$. The impulsive load to the tip of the 10th rib can be seen to excite principally the first bending mode of the rib. Figure 7 shows the maximum tip displacement of the individual ribs. Clearly by $\tau = 100$, all the ribs have been excited as is evidenced by their maximum tip displacements. The peak displacement in Fig. 7 occurs on the rib to which the impulse was applied. The other ribs never reach this magnitude because the energy becomes distributed among all the ribs. Note that although there is clearly a difference between the propagation in the perfect and imperfect structure in Fig. 7, all the ribs do become excited by $\tau = 100$, and the energy is clearly not confined to the vicinity of the impulsive load. This could be anticipated to some extent because a load at the tip would be expected to excite principally the first bending mode of the rib as is the case shown in Fig. 6 and the other modes to a lesser extent, and the first mode group, which is primarily first bending, is still extended. This explanation is verified by examining the coefficients of the mode shapes used in the Rayleigh-Ritz analysis that indicate that the dominant mode excited in the 10th rib is the first bending.

The affect of applying the impulsive load at another location along the rib is illustrated in Fig. 8 where the impulsive load is applied to the 10th rib at a distance of 0.3ℓ from the hub. This loading excites the second and third bending modes of the 10th rib as well as the first bending mode, as can be seen in Fig. 8 and by examining the coefficients in the Rayleigh-Ritz analysis. Figure 9 shows the maximum tip displacement for the impulse loading of Fig. 8. Once again, all the ribs are excited by $\tau = 100$, and there is not a significant difference between the imperfect and perfect structure with regard to the extent of the disturbance propagation as shown in Fig. 9. The actual details of the propagation are clearly different as seen in Fig. 8. Since the ribs are connected at their tips by a single axial member, the force transmitted from the rib with the loading will tend to excite the first rib bending mode of the adjacent ribs, even though the 10th rib clearly has strong second and third bending components. This can be seen in Fig. 9 where all the ribs other than the 10th rib are primarily in first bending.

If only one axial member is used to connect the ribs, its location can have a significant effect on the disturbance propagation as illustrated in Fig. 10. In Fig. 10 the axial member is connected at the center of each rib, and an impulsive load is applied to the center of the 10th rib. For the perfect structure, clearly all the ribs eventually become excited as shown in Fig. 10. For the imperfect structure, the displacements of the ribs farthest away from the source of excitation remain small, although all the ribs are excited to some extent. Calculations for $\tau = 10^6$ show very little change in the extent of propagation, suggesting the vibratory energy remains confined for all time. When the axial member is located at the center of the ribs, the first mode group was found to be no longer extended but rather was localized. A discussion on the effect of the constraint location on the degree of localization can be found in Ref. 9. The first bending mode was principally excited in the ribs adjacent to the rib to which the impulsive load was applied, and the location of the coupling member did not affect this significantly. The primary difference in the extent of propagation was due to the fact that the first mode was becoming localized.

The ribs of a reflector can be expected to have a weaker coupling out-of-plane since to the first order no mesh stresses are induced by the out-of-plane motions for a flat reflector.[14] To illustrate the effect of weaker coupling, the effective stiffness was reduced to $k^a = 0.03EI/\ell^3$, and an impulsive load was applied to the midpoint of the 10th rib. The connecting axial member was located at the tips of the ribs. The maximum tip displacements for this case are shown in Fig. 11 for $t < 10^5$. For the perfect structure, all the ribs eventually become ex-

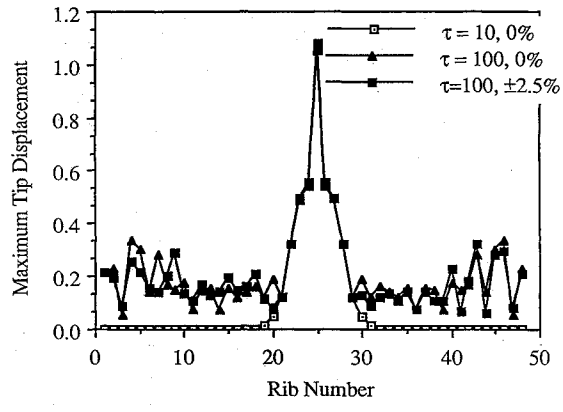

Fig. 14 The maximum displacement associated with impulsive loading of a 48-rib reflector with $k_a = 0.298\ EI/\ell^3$. Note that all the ribs of both the perfect and imperfect structures are excited by $\tau = 100$.

cited, whereas for the imperfect structure this is not the case, and the degree to which a rib is excited diminishes as a function of its distance from the rib originally excited. For this coupling strength, the modes in the first mode group were found to be no longer merely perturbed but rather were becoming localized. In Fig. 12, the $n = 0$ and 4 modes are shown for both the perfect and imperfect structures. Although the modes shown in Fig. 12 both have regions where the ribs are virtually unexcited, they are far from being "strongly" localized to one substructure. Figures 10 and 11 indicate that the important variable in determining the extent to which the impulsive load will propagate is the degree of localization of the first mode group, which is primarily the first bending mode, and the localization of the higher mode groups is not as important. When the first mode group does not localize, the impulsive load propagates throughout the structure and is not confined near the region of excitation. When the mode group is localized, all the ribs do not become excited to the same degree, and some confinement of the vibrations does appear to occur.

Results for a 48-rib reflector are shown in Figs. 13 and 14. The same coupling stiffness used for the 18-rib reflector was used in the 48-rib reflector. In this case, the addition of more ribs resulted in the severe distortion in some of the modes in the first group as shown in Fig. 13, in contrast to the slight distortion in the 18-rib case. In Fig. 13, the $n = 0$, 1, and 4 modes of the first mode group are shown. Note that while the $n = 0$ and 1 modes are highly distorted, the $n = 4$ mode is just slightly perturbed. In Fig. 14, the disturbance propagation associated with applying an impulsive load to the tip of the 25th rib is shown. The connecting axial member is located between the tip of the ribs. Note that all the ribs are excited by $\tau = 100$ in both the perfect and imperfect structure, and in this case, although the addition of more ribs resulted in distortion of modes in the first mode group, it was not sufficient to localize them to the extent that the energy becomes confined. To what extent the modes of a mode group need to be localized before the energy becomes confined has yet to be determined.

Conclusions

The following main conclusions can be drawn from this study for the generic class of large space reflectors with radial ribs:

1) If the first mode group (which is primarily first bending) is not localized, then the disturbance associated with impulsive loading of a single rib is found to propagate throughout both the perfect and imperfect structures regardless of where on the rib the impulse is applied. This is true even when the higher mode groups are strongly localized. The details of the propagation are different.

2) The first bending mode was principally excited in the ribs next to the one subjected to impulsive loading, even when the ribs were connected at a location other than the tip.

3) When the first mode group is localized (that is, extending over several substructures but not the whole structure), the disturbance associated with the impulsive loading of a single rib does not appear to propagate throughout the structure. The displacement of the ribs farthest away from the source of excitation remained small, although they were excited a small amount. To what degree the modes of the first mode group need to be localized remains to be determined.

References

[1]Anderson, M. S., and Williams, F. W., "Vibration and Buckling of General Periodic Lattice Structures," *Proceedings of the AIAA/ASME/ASCE/AHS 24th Structures, Structural Dynamics, and Materials Conference,* AIAA Paper 84-0979, AIAA, New York, May 1984, pp. 206–213.

[2]Bendiksen, O. O., "Mode Localization in Large Space Structures," *AIAA Journal,* Vol. 25, No. 9, 1987, pp. 1241–1248.

[3]Michimur, S., and Nagamatsu, A., "A Vibration Analysis of an Impeller: Use of the Cyclic Symmetry Method," *Theoretical and Applied Mechanics, The Proceedings of the 30th Japan National Congress for Applied Mechanics,* Vol. 30, 1980, pp. 313–321.

[4]Hodges, C. H., "Confinement of Vibration by Structural Irregularity," *Journal of Sound and Vibration,* Vol. 82, No. 3, 1982, pp. 411–424.

[5]Bendiksen, O. O., "Aeroelastic Stabilization by Disorder and Imperfections," XVI International Congress of Theoretical and Applied Mechanics, Paper No. 583P, Lyngby, Denmark, Aug. 1984.

[6]Pierre, C., "Analysis of Structural Systems with Parametric Uncertainties," Ph.D. Dissertation, Dept. of Mechanical and Aerospace Engineering and Materials Science, Duke Univ., Durham, NC, July 1985.

[7]Pierre, C., Tang, D. M., and Dowell, E. H., "Localized Vibrations of Disordered Multispan Beams: Theory and Experiment," *AIAA Journal,* Vol. 25, No. 9, 1987, pp. 1249–1257.

[8]Cornwell, P. J., and Bendiksen, O. O., "Localization of Vibrations in Large Space Reflectors," *AIAA Journal,* Vol. 27, No. 2, 1989, pp. 219–226.

[9]Pierre, C., and Cha, P., "Strong Mode Localization in Nearly Periodic Disordered Structures," *AIAA Journal,* Vol. 27, No. 2, 1989, pp. 227–241.

[10]Kissel, G. J., "Localization in Disordered Preiodic Structures," AIAA Paper 87-0819, April 1987.

[11]Pierre, C., "Weak and Strong Vibration Localization in Disordered Structures: A Statistical Investigation," *Journal of Sound and Vibration,* Vol. 138, No. 2, 1990.

[12]Hodges, C H., and Woodhouse, J., "Vibration Isolation from Irregularity in a Nearly Periodic Structure: Theory and Measurements," *Journal of the Acoustical Society of America,* Vol. 74, No. 3, 1983, pp. 894–905.

[13]El-Raheb, M., and Wagner, P., "Static and Dynamic Characteristics of Large Deployable Space Reflectors," *Proceedings of the AIAA/ASME/ASCE/AHS 22nd Structures, Structural Dynamics and Materials Conference,* AIAA Paper 81-0503, AIAA, New York, April 1981, pp. 77–84.

[14]Schaechter, D. B., "Free Vibration Continuum Model for a Flexible, Wrap-Rib Antenna," *Journal of the Astronautical Sciences,* Vol. 33, No. 1, 1985, pp. 3–14.

Earl A. Thornton
Associate Editor

JOURNAL OF SPACECRAFT AND ROCKETS
Vol. 29, No. 4, July-August 1992

Oscillatory Instabilities in a Rapidly Rotating Liquid Annulus

J. A. Szymczyk,* J. Siekmann,† and J. T. Cieśliński‡
University of Essen, Essen, Germany

Under low-gravity conditions, rotating fluid systems having liquid-solid, liquid-liquid, or liquid-gas interfaces with imposed (horizontal or vertical) temperature gradients are significantly influenced by thermal Marangoni effects. The flow within a rapidly rotating liquid cylinder with a free inner surface that is caused by a vertically applied temperature gradient is considered. The liquid-gas zone was heated from above and cooled from below. The onset of thermocapillary convection is investigated and the flow pattern at the interface as a function of the Marangoni number and the rotational speed for two liquids having different Prandtl numbers is analyzed. The topological flow structures are discussed in some detail.

Nomenclature

a = thermal diffusivity, m^2/s
Bo = Bond number—ratio of the centrifugal force to the surface tension force, $\rho_o \cdot \Omega^2 \cdot R^3/\sigma_o$
E = Ekman number—ratio of the viscous force to the Coriolis force in the liquid-gas zone, $\nu/\Omega \cdot R^2$
Fr = Froude number—ratio of the centrifugal force to the gravitational force, $\Omega^2 \cdot R/g$
g = acceleration due to gravity, m/s^2
H = height of the liquid-gas interface, m
Mg = Marangoni number—ratio of a force due to a surface tension gradient to the viscous force, $|\partial\sigma/\partial T| \cdot H \cdot \Delta T/(\mu \cdot a)$
Pr = Prandtl number—ratio of viscous diffusivity to thermal diffusivity, ν/a
R = radius, m
r = radial coordinate, m
T = temperature, K
Ta = Taylor number—ratio of the Coriolis force to the viscous force, $Ta^{1/2} = 2 \cdot \Omega \cdot H^2/\nu$
T_C = temperature of the cold wall, K
T_H = temperature of the hot wall, K
z = axial coordinate, m
ΔT = temperature difference, $T_H - T_C$, K
Θ = angular coordinate, rad
μ = dynamic viscosity, Ns/m^2
ν = kinematic viscosity, m^2/s
ρ_o = density, kg/m^3
σ = surface tension, N/m
Ω = angular velocity, rad/s

I. Background

A. Rotating Fluid Systems

CONVECTION in rotating fluids caused by an applied temperature gradient has been studied both experimentally and theoretically for a sufficiently wide range of the determining parameters. Without demanding completeness, Fig. 1 presents the representative works on convection and thermocapillary flow under rotation for different flow configurations and thermal conditions. One can differentiate four basic typical configurations: 1) horizontal fluid layers between two infinite plates (this case is of theoretical importance only)[1,2]; 2) liquid bridges, serving as simulated floating-zone configurations in crystal growth from the melt[3-5]; 3) containers completely filled with fluid having a free[6] or rigid surface[7] with insulated or perfectly conducting sidewalls[8] and different cross sections,[8] sometimes with an additional rotating lid[9]; and 4) annulus with solid outer and inner surfaces and different cross sections,[10,11] or with a rigid sidewall and free inner surface (so-called inverse liquid bridge).[12] In the case of a lack of a temperature gradient, fluid and container must rotate with the same constant angular velocity.

The rotating fluid system used in this investigation is shown in Fig. 2. It consisted of an annulus with a free inner liquid-air interface produced by the rotation of a transparent glass cell with a constant angular velocity. A cylindrical coordinate system (r, Θ, z) is used to describe this system, where the z axis coincides with the symmetry axis of the zone. The volume ratio for which the experiments have been conducted, i.e., $V_{fluid}/V_{chamber}$, was 0.5. The aspect ratio (altitude/diameter, H/D) was 1. The experimental chamber was rotated at various speeds of rotation, i.e., Ω = 62.83-104, 30 rad/s (600-1000 rpm).

The driving force for flows in this rotating cylindrical fluid system is the nonuniform temperature field. It produces variations of the fluid density and the surface tension at the fluid-fluid interface. As an effect of density variations, gravitational-buoyancy-driven motion occurs through the vertical gravitational force and centrifugal-buoyancy-driven motion produced by the radial centrifugal force. As an effect of surface tension variations, there results a thermocapillary convection. These three types of motion cannot be studied independently since they are closely coupled.

B. Linear Dynamics of Rotating Stratified Fluids

The flow in the rotating liquid-gas zone with a free inner surface is influenced by thermocapillary convection, gravitational and centrifugal buoyancy, and the motion of the solid container. Because of small Ekman numbers (herein, E is of the order 10^{-3}), the fluid motion with a free inner surface in the rotating cylinder is composed of four parts: a core motion, Ekman layers on the top and the bottom plates, a sidewall layer, and a side layer at the liquid-gas interface.

The dynamics of rotating fluids depends on stratification. For weak stratification, the fluid, in all regions, acts as if it were homogeneous, i.e., its interior dynamics is strongly controlled by the Ekman-layer suction. The Taylor-Proudman theorem is valid in the interior, and the sidewall layer[13,14] has a double structure and is made up of an inner Stewartson boundary layer of thickness $E^{1/3}$ in which viscous and Coriolis forces balance and an outer Stewartson $E^{1/4}$ layer,[15] which serves to match the fluid velocity to that of the vertical boundary layer. The thermocapillary flow at the liquid-gas interface

Presented in part as Paper 90-0410 at the AIAA 28th Aerospace Sciences Meeting, Reno, NV, Jan. 8-11, 1990; received March 29, 1990; revision received Sept. 3, 1990; accepted for publication March 15, 1991.

*Member of Scientific Staff, Chair of Mechanics.
†Professor, Chair of Mechanics. Member AIAA.
‡Member of Scientific Staff, on leave from the Technical University Gdańsk, Poland, Chair of Thermodynamics.